

Three-dimensional imaging of colloidal glasses under steady shear

R. Besseling¹, Eric R. Weeks², A. B. Schofield¹, W. C. K. Poon¹

¹Scottish Universities Physics Alliance (SUPA) and School of Physics,

The University of Edinburgh, Kings Buildings, Mayfield Road, Edinburgh EH9 3JZ, United Kingdom.

² Physics Department, Emory University, Atlanta, Georgia 30322, USA.

(Dated: December 2, 2024)

Using fast confocal microscopy we image the three-dimensional dynamics of particles in a yielded colloidal hard sphere glass under steady shear. The structural relaxation, observed in regions with uniform shear, is nearly isotropic but distinctly different from that of a quiescent meta-stable liquid. The inverse relaxation time τ_α^{-1} and diffusion constant D , as functions of the *local* shear rate $\dot{\gamma}$, show marked shear thinning behavior with $\tau_\alpha^{-1} \propto D \propto \dot{\gamma}^{0.8}$ over more than two decades in $\dot{\gamma}$. In contrast, the *global* rheology of the system displays Herschel-Bulkley behavior and we attribute this difference to shear localization seen on larger scales and the existence of a *static* yield stress.

PACS numbers: 82.70.-y, 83.50.-v, 83.80.Hj

Glassy materials are ubiquitous in nature and in industry, ranging from molecular and metallic glasses [1, 2] to soft glasses like colloidal suspensions, emulsions and foams [3, 4]. Of special importance, both practically and fundamentally, is their rheological behavior: while their microstructure is disordered and liquid-like, mechanically they are solids, with finite shear moduli and yield stresses and with complex nonlinear behavior when pushed beyond the yielding transition.

Among the many open issues in this nonlinear glassy rheology, steady state flow stands as the simplest example, yet far from being fully understood. Theories [4, 5, 6, 7] have invoked various mechanisms through which shear causes relaxation of initially arrested structures, with predictions for constitutive laws ranging from powerlaw fluid to dynamic yield stress behavior, all assuming globally uniform shear. Simulation studies, so far the main tool to directly check the relation between microscopic behavior and macroscopic flow, revealed spatially heterogeneous relaxation [7, 8] and strong shear thinning [9, 10]. However, experiments are only beginning to address microscopic dynamics under shear, and have been restricted to coarse grained information, two dimensional (2D) or interrupted flows, or ordering phenomena [11, 12, 13, 14]. Moreover, experiments imaging the *global* flow [15] showed that soft glasses often exhibit shear localization, which can not be described with a simple constitutive law. This was also observed in boundary driven simulations of a Lennard-Jones (LJ) glass [16].

In this Letter we report on three-dimensional (3D) imaging of the microscopic relaxation in a sheared colloidal glass. The relaxation is nearly isotropic but different from that of supercooled liquids. The inverse relaxation rate τ_α^{-1} and the diffusion constant D show marked shear thinning as function of the *local* shear rate $\dot{\gamma}$ in our imaged volume: $\tau_\alpha^{-1} \propto D \propto \dot{\gamma}^{0.8}$. This local behavior contrasts the global rheology of the system, which can be attributed to the coexistence of sheared and jammed regions in the global flow.

We use sterically-stabilized polymethylmethacrylate (PMMA) particles (radius $a = 850\text{nm}$, determined by

light scattering, polydispersity $\lesssim 10\%$ [17]) fluorescently labelled with nitrobenzoxadiazole, suspended in a mixture of cycloheptyl bromide and decalin (viscosity $2.6\text{ mPa}\cdot\text{s}$) for both density and refractive index matching. In this medium particles acquire a small charge [18] which is largely screened by adding 4 mM tetrabutylammonium chloride, giving nearly hard-sphere (HS) behavior, with a glass transition at volume fraction $\phi_g \simeq 0.58$ (determined from mean-squared displacements) [19]; we work at $\phi \simeq 0.62$ (determined by imaging). The dimensionless shear rate, or Peclet number, is $\text{Pe} = 4a^2\dot{\gamma}/D_0 = 24\dot{\gamma}\tau_B$, with D_0 the bare diffusion coefficient and $\tau_B = a^2/6D_0 = 1.24\text{ s}$ the Brownian time in our system. Our experiments cover the range $0.005 \lesssim \text{Pe} \lesssim 1$.

We employ a linear parallel plate shear-cell with a plate separation $\sim 400 - 800\text{ }\mu\text{m}$, parallel to $\pm 5\mu\text{m}$ over a $\sim 200\text{ mm}^2$ drop confined between the plates by surface tension. x , y and z denote the velocity, vorticity (or neutral) and gradient directions respectively. The top plate is driven at $0.05 - 10\text{ }\mu\text{m/s}$ by a mechanical actuator with magnetic encoder, and steady shear is applied for a finite, but long, time. The maximum total accumulated shear is limited by cell design to $\Delta\gamma \lesssim 1000\%$. Boundary slip, present when using bare glass slides, was prevented by coating the slides with particles (1 – 3 disordered monolayers) [20]. A solvent bath minimized evaporation.

A $30 \times 30 \times 15\text{ }\mu\text{m}^3$ volume in the drop (containing $N \sim 3000$ particles) was imaged from below as a stack of 75 slices using a fast confocal microscope (VT-Eye, Visitech International). The scanning of each 3D stack took $\sim 2\text{ s}$. In each stack, particles were located with resolution $\delta x, \delta y \sim 30\text{ nm}$ and $\delta z \sim 90\text{ nm}$ [21]. Tracking from frame to frame was achieved by first subtracting from the raw coordinates a time (t) dependent x -displacement profile, measured via correlation analysis of raw images, and adding this back after particle tracking. The resulting x -displacements over a given time interval dt , $\{\Delta x_i(z_i, dt)\}$ ($i = 1$ to N), always have an average linear dependence on z . From this we checked that the sample in our imaged volume was indeed subjected to uniform shear, and measured the actual shear rate $\dot{\gamma}$, which may differ from the

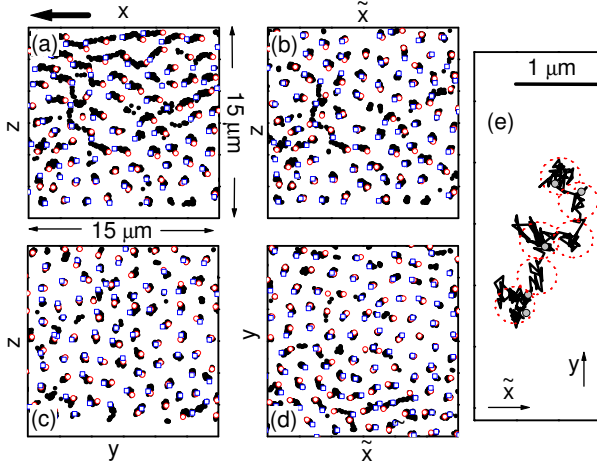


FIG. 1: Particle trajectories for $\dot{\gamma} = 0.93 \times 10^{-3} \text{ s}^{-1}$. (a) 1.5 μm thick slice in the x,z plane over 160 s; the start of the trajectories is shown by red circles; the end by blue squares. The big arrow marks the shear direction. (b) As in (a) but in the desheared, \tilde{x}, z , reference frame, with $\tilde{x}_i = x_i - \dot{\gamma} \int_0^t z_i(t') dt'$. (c) y, z plane over 160 s. (d) \tilde{x}, y plane over 160 s. (e) Single trajectory in the \tilde{x}, y plane over 800 s. Dotted circles indicate rattling in several cages (not the particle size), grey dots mark the locations at $t = 0, 200, 400, 600, 800$ s.

applied rate $\dot{\gamma}_a$ due to shear localization. We will come back to this in the conclusion and elsewhere; for now we mention that we focus on steady states with a linear velocity profile in a region from $15 - 30 \mu\text{m}$ above the cover slide, while, when present, strong decay in the shear rate (near a jammed region) occurs at least $\Delta z \sim 20a$ away from the considered region. We also checked, via bond-order analysis [22], that shear-induced crystallization [23] was absent for our range of $\dot{\gamma}$.

Figure 1(a) shows the trajectories in an x,z slice at $\dot{\gamma} = 0.93 \times 10^{-3} \text{ s}^{-1}$. The displacement gradient due to shear is evident. To highlight the shear-induced dynamics, we show in Fig. 1(b) the *non-affine* component of the motion obtained by subtracting the uniform shear via $\tilde{x}_i = x_i - \dot{\gamma} \int_0^t z_i(t') dt'$. Considerable shear-induced non-affine displacements are seen in this plane as well as in the other planes, Figs. 1(c,d). On the time scale considered here, these rearrangements are heterogeneous, somewhat similar to observations in *quiescent* systems in the supercooled liquid state, $\phi < \phi_g$ [24]. Zooming in on a single particle, Fig. 1(e), we observe that its dynamics under shear consists of intervals of cage ‘rattling’, interrupted by shear-induced plastic cage-breaking events.

Next, we study the relaxation via the incoherent scattering function, $F_s(Q, t) = \langle \cos(Q[y_i(t_0+t) - y_i(t_0)]) \rangle_{i,t_0}$, at a scattering vector $Q = Q_m \simeq 3.8a^{-1}$ (the peak in the structure factor $S(Q)$ obtained from the data). In Fig. 2 we show a selection of the results for $\vec{Q} \parallel y$ (the neutral direction), but the results (not shown) for $\vec{Q} \parallel z$ and x (using the non-affine displacements \tilde{x}_i for the latter) are similar. F_s for the quiescent glass ($\dot{\gamma} = 0$) hardly de-

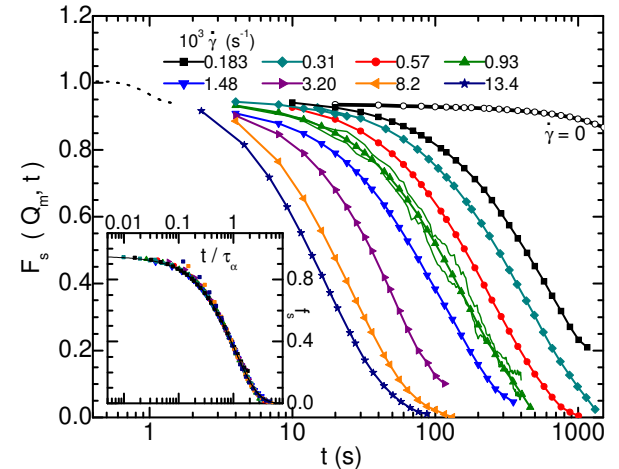


FIG. 2: Selected incoherent scattering functions, $F_s(Q_m, t)$, with $\dot{\gamma}$ increasing from right to left. The thin lines for $\dot{\gamma} = 0.93 \times 10^{-3} \text{ s}^{-1}$ represent two of the curves used in the average, with time origins t_0 separated by 180s ($\sim 1.2\tau_\alpha$). The dashed line schematically indicates initial relaxation. Inset: master curve $f_s(Q_m, t/\tau_\alpha)$, showing collapse of F_s for all rates after scaling time by $\tau_\alpha(\dot{\gamma})$. Drawn line: $f_s \propto \exp(-t/\tau_\alpha)$.

cays over our observation window, reflecting the caging of particles by their neighbors; at longer times we observed aging, as in other studies [14, 25]. The short time decay due to initial cage exploration ($t \lesssim \tau_B$ [26], dashed line in Fig. 2) is inaccessible in our experiments. At small $\dot{\gamma}$, F_s at short times still exhibits a plateau, in agreement with the caging seen in Fig. 1(e). As $\dot{\gamma}$ increases, this plateau shrinks and for the highest $\dot{\gamma}$ it vanishes and likely merges with the short time decay. At longer times, F_s decays strongly for all $\dot{\gamma} \neq 0$, marking shear-induced structural relaxation and cage rearrangements. The structural, or α , relaxation time τ_α , defined by $F_s(Q_m, t = \tau_\alpha) = e^{-1}$, decreases on increasing $\dot{\gamma}$. Importantly, F_s is independent of the starting time t_0 (see data for $\dot{\gamma} = 0.93 \times 10^{-3} \text{ s}^{-1}$), i.e., a stationary state is achieved.

A theoretical prediction for the behavior of F_s is the so-called time-shear superposition principle [5, 6]: when time is scaled by τ_α , the α -relaxation should follow a master curve $f_s(Q, t/\tau_\alpha)$. Our data indeed show this scaling (Fig. 2 inset), with f_s best described by a pure exponential, similar to the simulations in [9], but different from the stretched relaxation seen for $\phi < \phi_g$ and $\dot{\gamma} = 0$ [26].

We now consider the shear rate dependence of τ_α . As shown in Fig. 3(a), the relaxation time, collected for all data [27], exhibits pronounced shear thinning with $\tau_\alpha \propto \dot{\gamma}^{-\nu}$ and $\nu = 0.80 \pm 0.01$. This behavior is insensitive to the criterion or Q used to determine τ_α . A direct consequence of this power law is that the accumulated strain at τ_α is not constant but varies as $\dot{\gamma}\tau_\alpha \propto \dot{\gamma}^{0.2}$, suggesting that, over the present data range, additional relaxation channels open up on reducing $\dot{\gamma}$. We discuss below the rheological implications this may have and compare the result with theoretical models.

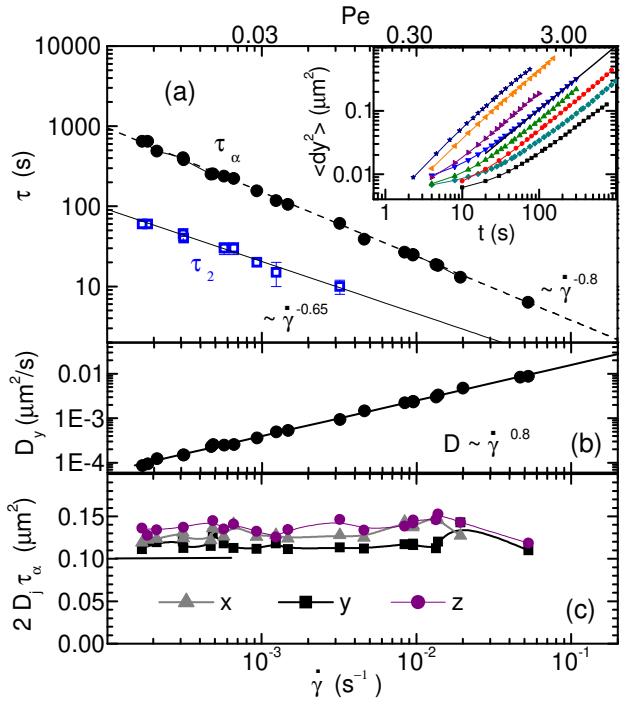


FIG. 3: (a) Structural relaxation time (\bullet) and the characteristic time τ_2 for the crossover from caged to diffusive behavior (\square) vs. $\dot{\gamma}$; dashed line: $\tau_\alpha \propto \dot{\gamma}^{-0.8}$; full line: $\tau_2 \propto \dot{\gamma}^{-0.65}$. Inset: mean square displacement in the vorticity direction for shear rates as in Fig. 2. Line: $\langle dy^2(t) \rangle = 2D_y t$ for $\dot{\gamma} = 1.48 \times 10^{-3} \text{ s}^{-1}$. (b) (\bullet) Diffusion constant D_y vs. $\dot{\gamma}$. Line: $D_y \propto \dot{\gamma}^{0.8}$. (c) The scaled diffusion constant $2D_j \tau_\alpha \simeq \langle dr_j^2(\tau_\alpha) \rangle$ vs. $\dot{\gamma}$ for $j = x, y, z$. Line: the value $\langle dy^2(\tau_\alpha) \rangle = 2/Q_m^2$ as expected for gaussian behavior.

Turning to the mean squared displacement, the inset to Fig. 3(a) shows $\langle dy^2(t) \rangle$ for selected rates. It exhibits a crossover from caged to diffusive motion for $\sqrt{\langle dy^2 \rangle}/a \simeq 0.15$ ($\langle dy^2 \rangle \simeq 0.016 \text{ } \mu\text{m}^2$), in reasonable agreement with the ‘Lindemann parameter’ measuring the cage rattling at the quiescent glass transition [19]. The long time diffusion constant D_y , Fig. 3(b), follows the relaxation rate $D_y \propto \tau_\alpha^{-1} \propto \dot{\gamma}^{0.8}$, and *not* the shear rate $\dot{\gamma}$. To show this more clearly and also address the anisotropy in the dynamics, we plot in Fig. 3(c) the product $2D_j \tau_\alpha$ for the three directions ($j = x, y, z$) along with the value $\langle dy^2(\tau_\alpha) \rangle = 2/Q_m^2$ expected from a gaussian approximation $F_s(Q_m, t) \simeq e^{-Q_m^2 \langle dy^2(t) \rangle / 2}$ [26]. The value for $2D_y \tau_\alpha$ agrees well with $2Q_m^{-2}$ and this gaussian long time behavior also occurs in the other directions [29]. We again note the difference with *quiescent* samples for $\phi < \phi_g$, where we always find $D\tau_\alpha < Q^{-2}$ for $Q \geq Q_m$. Figure 3(c) also shows that the diffusion constants exhibit only a mild anisotropy: while $D_z > D_{x,y}$, the difference is at most $\sim 20\%$. Similar or even smaller anisotropy has been observed in various simulations of sheared, glassy systems [8, 10]. Moreover, isotropic shear-induced diffusion is also observed in *dilute* suspen-

sions [30]. However, sheared *non-Brownian* suspensions ($\text{Pe} \rightarrow \infty$) show a marked anisotropy ($D_x^\infty / D_{y,z}^\infty \sim 8$) [31], with D^∞ simply proportional to the shear rate.

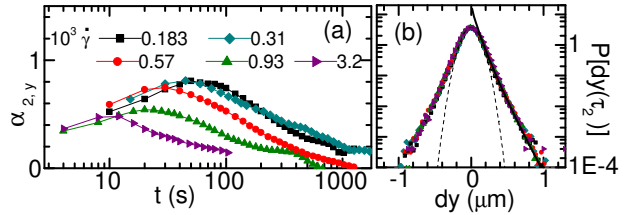


FIG. 4: (a) Nongaussian parameter $\alpha_2(t)$ of the probability distribution $P[dy(t)]$ of y -displacements, for several $\dot{\gamma}$. (b) $P[dy(\tau_2)]$ at $t = \tau_2(\dot{\gamma})$ for the corresponding $\dot{\gamma}$, showing a near collapse of the data (each involving $> 10^5$ displacements). Dashed line: best gaussian fit. Full line: $P \propto \exp(-Ady^{0.8})$.

As a last characterization of the microscopic dynamics we study the probability distribution of the displacements $P(dy(t))$ and the non-gaussian parameter $\alpha_{2,y} = \langle dy^4(t) \rangle / 3 \langle dy^2(t) \rangle^2 - 1$. The latter measures the contribution of broad, non-gaussian, tails to $P(dy(t))$, reflecting cage rearranging motions such as in Fig. 1(e). Figure 4(a) shows $\alpha_{2,y}(t)$ for various $\dot{\gamma}$. It exhibits a peak for $t \equiv \tau_2$ corresponding to the crossover from caged to diffusive behavior in the MSD (inset, Fig. 3(a)), and vanishes for $t \gtrsim \tau_\alpha$. A non-zero α_2 also suggests cooperative motion and is consistent with the heterogeneous trajectories for $t \lesssim \tau_\alpha$ in Fig. 1 (b)-(d). A detailed account of these heterogeneities will be given elsewhere. We do mention here that the peak time follows $\tau_2 \propto \dot{\gamma}^{0.65}$ (Fig. 3(a)), somewhat different from the τ_α scaling. More interesting, the distributions $P[dy(t = \tau_2(\dot{\gamma}))]$ display a near collapse for different shear rates (Fig. 4(b)), despite a slight decrease of $\alpha_2(\tau_2)$ with $\dot{\gamma}$ [32]. In quiescent systems at $\phi < \phi_g$, such (near) collapse of $P[dy(\tau_2(\phi))]$ at different ϕ is *not* expected since there $\alpha_2(\tau_2)$ increases *strongly* with ϕ while the MSD at τ_2 decreases rapidly [24].

Finally, we return to the shear thinning behavior $\tau_\alpha(\dot{\gamma})$ and explicitly address the rheology of our system. Identifying τ_α as a measure for the viscosity [6] and hence a dimensionless stress as $\bar{\sigma} \propto \dot{\gamma} \tau_\alpha(\dot{\gamma})$ [28], we obtain a ‘microscopic’ flow curve $\bar{\sigma} \propto \dot{\gamma}^{0.2}$ exhibiting power-law fluid behavior over our range (Fig. 5). Recent theories [4, 6] argued for the existence of a dynamic yield stress $\sigma(\dot{\gamma} \rightarrow 0) = \sigma_Y$ in sheared glasses. While the specific predictions in [6] were verified via simulations of an LJ glass [28], our experimental data show no sign of a plateau in $\bar{\sigma}$ for reduced rates down to $\text{Pe} \simeq 0.005$. Instead, the data agree with a schematic model for driven glasses in [5] and, interestingly, also match the ‘creep’ behavior of a driven particle in a correlated random potential [33].

Let us then turn to the *macroscopic* rheology of our system: shown in Fig. 5 is the global relation of stress σ versus average shear rate $\dot{\gamma}_a$, measured using a stress controlled rheometer (AR2000, TA Instr.) in cone-plate geometry (diameter 40 mm, angle 1°, both surfaces coated

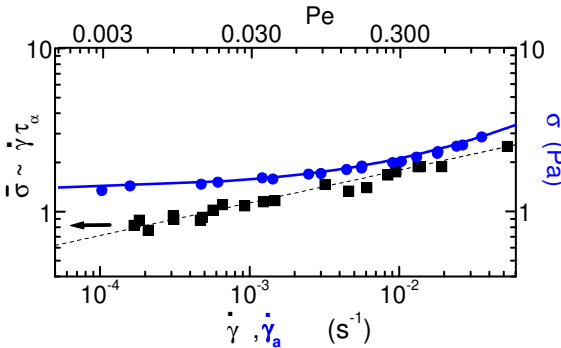


FIG. 5: (■) Local 'flow curve' $\bar{\sigma} \propto \dot{\gamma}\tau_\alpha$ vs. $\dot{\gamma}$ (dashed line: $\bar{\sigma} \propto \dot{\gamma}^{0.2}$) compared with the macroscopic flow curve $\sigma(\dot{\gamma}_a)$ measured in cone-plate geometry (circles). The drawn line is a fit based on the Herschel-Bulkley model (see text).

with particles). It is described by $\sigma(\dot{\gamma}_a) = \sigma_Y + A\dot{\gamma}_a^n$ with $\sigma_Y = 1.36$ Pa, $n = 0.56$, with *apparent* dynamic yield stress behavior similar to previous studies of HS glasses [34], but different from our microscopic observation. However, as mentioned, the system shows shear localization in which a global shear rate $\dot{\gamma}_a$ typically corresponds to a coexisting jammed region ($\dot{\gamma} \simeq 0$) and a flowing region with $\dot{\gamma} > \dot{\gamma}_a$. Preliminary experiments

imaging the flow *inside* the rheometer indeed show that such localization sets in for $\dot{\gamma}_a \simeq 10^{-2}$ s $^{-1}$ and is more pronounced for smaller $\dot{\gamma}_a$. The inhomogeneous flow may be attributed to the existence of a *static* yield stress $\sigma_y > \sigma_Y$, making the *total* flow curve multivalued for small $\dot{\gamma}$. The resulting picture, with powerlaw fluid behavior in steady shear but a finite, *static* yield stress is consistent with the model in [5], but further studies are required to understand its possible universality.

In conclusion, we image 3D microscopic relaxation in a colloidal glass under steady shear. The relaxation occurs in 'fluidized' bands, in which we observe nearly isotropic 'cage breaking' dynamics which differs from that in supercooled liquids. The relaxation rate depends as a power law on the *local* shear rate: $\tau_\alpha^{-1} \propto \dot{\gamma}^{0.8}$. This microscopic shear thinning is contrasted with the global rheology of the glass and the difference attributed to shear localization seen in the system. Our 3D imaging under shear presents a novel route to study microscopic dynamics in driven soft glasses and allows to address a variety of fundamental questions in the flow of these systems.

We thank J. Bergenholz, M. E. Cates, M. Fuchs, P. Pusey, G. Petekidis and L. Isa for helpful discussions. UK and US work was funded by EPSRC GR/S10377/01 and NSF Grant No. DMR-0239109 respectively.

[1] M.D. Ediger *et al.*, J. Phys. Chem. **100**, 13200 (1996).
[2] M. Heggen *et al.*, J. Appl. Phys. **97**, 033506 (2005); H. Kato *et al.*, Appl. Phys. Lett. **73**, 3665 (1998).
[3] R.G. Larson, *The Structure and Rheology of Complex Fluids* (Oxford University Press, New York, 1999).
[4] P. Sollich *et al.*, Phys. Rev. Lett. **78**, 2020 (1997).
[5] L. Berthier, J. Phys. Cond. Mat. **15**, 933 (2003).
[6] M. Fuchs and M.E. Cates, Phys. Rev. Lett. **89**, 248304 (2002); Far. Disc. **123**, 267 (2003). K. Miyazaki and D.R. Reichman, Phys. Rev. E **66**, 050501(R) (2002).
[7] M.L. Falk and J.S. Langer, Phys. Rev. E **57**, 7192 (1998).
[8] R. Yamamoto and A. Onuki, Phys. Rev. E **58**, 3515 (1998); Phys. Rev. Lett. **81**, 4915 (1998).
[9] L. Berthier and J.L. Barrat, J. Chem. Phys. **116**, 6228 (2002); F. Varnik *et al.*, *ibid.* **125**, 164514 (2006).
[10] K. Miyazaki *et al.*, Phys. Rev. E **70**, 011501 (2004).
[11] G. Petekidis *et al.*, Phys. Rev. E **66**, 051402 (2002).
[12] P. Hebraud *et al.*, Phys. Rev. Lett. **78**, 4657 (1997).
[13] J. Lauridsen *et al.*, Phys. Rev. Lett. **93**, 018303 (2004). P. Varadan and M.J. Solomon, J. Rheol. **47**, 943 (2003); D. Derk *et al.*, J. Phys. Cond. Mat. **16**, 3917 (2004); I. Cohen *et al.*, Phys. Rev. Lett. **93**, 046001 (2004).
[14] D. Bonn *et al.*, Phys. Rev. Lett. **89**, 015701 (2002).
[15] P. Coussot *et al.*, Phys. Rev. Lett. **88**, 218301 (2002); L. Bégu *et al.*, Phys. Rev. Lett. **96**, 138302 (2006).
[16] F. Varnik *et al.*, Phys. Rev. Lett. **90**, 095702 (2003).
[17] This was deduced from the very slow crystallization of the quiescent samples for $\phi \gtrsim 50\%$.
[18] A. Yethiraj, A. van Blaaderen, Nature **421**, 513 (2003).
[19] The long-time rms-displacement at ϕ_g is $\sqrt{\langle dy^2 \rangle}/a \simeq 0.13$; the HS value is $\simeq 0.18$ [26].
[20] The coating also suppresses wall induced ordering as may occur in glassy suspensions near untreated surfaces.
[21] J.C. Crocker and D.G. Grier, J. Col. Int. Sc. **179**, 298 (1996). At our frame rate, shear-induced distortions in the x, z plane are unimportant for $\dot{\gamma} \lesssim 0.05$ s $^{-1}$.
[22] P.R. ten Wolde *et al.*, J. Chem. Phys **104**, 9932 (1996); The average number of crystalline bonds per particle was $\langle N_x \rangle \sim 2.5$ and constant in time, with only small (fluctuating) clusters of crystalline particles (with $N_x \geq 8$).
[23] B.J. Ackerson and P.N. Pusey, Phys. Rev. Lett. **61**, 1033 (1988); M.D. Haw *et al.*, Phys. Rev. E **57**, 6859 (1998). We observed (partial) crystallization for faster ($\dot{\gamma} \gtrsim 0.1$ s $^{-1}$) shear, either steady or sawtooth oscillatory shear with a strain amplitude $\sim 100\%$.
[24] E.R. Weeks *et al.*, Science **287**, 627 (2000); W.K. Kegel and A. van Blaaderen, Science **287**, 290 (2000).
[25] R.E. Courtland and E.R. Weeks, J. Phys. Cond. Mat. **15** S359 (2003).
[26] W. van Megen *et al.*, Phys. Rev. E **58**, 6073 (1998).
[27] Fig. 3(a) includes two τ_α results at lower ϕ , $\phi[10^3\dot{\gamma} = 0.47$ s $^{-1}] \simeq 61\%$ and $\phi[10^3\dot{\gamma} = 1.48$ s $^{-1}] \simeq 60\%$, but they remarkably follow the same function $\tau = 0.6\dot{\gamma}^{0.6}$.
[28] F. Varnik, O. Henrich, Phys. Rev. B. **73**, 174209 (2006).
[29] Taking $\tau_{\alpha,j}$ evaluated from $F_s(Q_m \parallel j, t = \tau_{\alpha,j}) = 1/e$, yields $D_j \tau_{\alpha,j} \simeq 0.11$ independent of j .
[30] X. Qiu *et al.*, Phys. Rev. Lett. **61**, 2554 (1988).
[31] V. Breedveld *et al.*, J. Chem. Phys. **116**, 10529 (2002).
[32] Part of the variation in $\alpha_2(\tau_2(\dot{\gamma}))$ may be nonsystematic, associated with scatter in $P(dy)$ for large dy .
[33] H. Horner, Z. Phys. B **100**, 243 (1996).
[34] G. Petekidis *et al.*, J. Phys. Cond. Mat. **16**, 3955 (2004).